Impact of Bond Order Loss on Surface and Nanosolid Mechanics

Chang Q. Sun,*,† S. Li,‡ and C. M. Li†

School of Electrical and Electronic Engineering, Nanyang Technological University, Singapore 639798, Singapore, and School of Materials Science and Engineering, The University of New South Wales, Sydney NSW2052, Australia

Received: September 10, 2004; In Final Form: October 13, 2004

An analytical solution shows that a competition between bond order loss and the associated bond strength gain of the lower coordinated atoms near the edge of a surface dictates the mechanics of the surface and, hence, a nanosolid. Bond order loss lowers the activation energy for atomic dislocation, whereas bond strength gain enhances the energy density or mechanical strength in the region near the surface. Therefore, the surface is harder than the bulk interior at temperatures far below the melting point (T_m), and the surface becomes softer at temperatures close to the surface T_m that drops because of bond order loss. Matching predictions to measurements reveals that a transition happens to the Hall−Petch relationship for a nanosolid when the effect of bond order loss becomes dominant, and the critical size of the Hall−Petch transition depends intrinsically on the bond nature of the specimen and the ratio of T/T_m, where T is the temperature of operation.

I. Introduction

The unusual behavior of a surface and a nanosolid in mechanical strength such as hardness (P, also yield strength or flow stress), Young's modulus (Y), and compressibility (β, also ductility or extensibility) has been a subject of intensive study during past decades because of both fundamental and technological significance. The enhanced mechanical strength and Young's modulus of a surface and a nanosolid have been widely reported with debating mechanisms. For example, the hardness of nanocrystalline and microcrystalline pure nickel varies not only with the geometrical shapes (conical, Berkovich, and cube-corner) of the indenter tips but also with the strain rate in measurement, although the former is more significant. The maximal hardness that is peaked at a surface depth of ∼5 nm varies in the range 6−20 GPa with the tip shapes, but the peak position (5 nm depth) changes with neither the shapes of tips nor the strain rate.[1] Both the Y and P values of nitrogen-doped amorphous carbon films also show maximal hardness near the surface. The maximal hardness is ∼3−4 times higher than bulk values, whereas the peak positions in the hardness depth profiles remain unchanged when the nitrogen content or film thickness is varied.[2] Surfaces of Ag, Ni, Cu, and Al thin films are 4 ± 0.5 times harder than the bulk, and the hardness of α_2-TiAl and γ-TiAl surfaces are ∼2 times the corresponding bulk values.[3] The hardness of Ti, Zr, and Hf carbide films on silicon substrate increases from the bulk value of 18 to 45 GPa when the film thickness is decreased from 9000 to 300 nm.[4] By squeezing Si nanospheres of different sizes between a diamond-tipped probe and a sapphire surface, Gerberich et al.[5] determined at room temperature that a defect-free silicon nanosphere with a diameter of 40 nm is ∼4 times (50 GPa) harder than bulk silicon (12 GPa). The smaller the sphere, the harder it was: spheres with a diameter of 100 nm had a hardness of around 20 GPa. The Young's modulus of nanograined steel was determined to increase from 218 to 270 GPa associated with lattice contraction from 0.2872 to 0.2864 nm when the grain size is reduced from 700 to 100 nm.[6]

The mechanical strengthening with grain refinement in the size range of 100 nm or larger has traditionally been rationalized with the so-called T-unapparent Hall−Petch relationship (HPR)[7] that can be simplified in a dimensionless form normalized by the bulk strength, $P(0, T)$, measured at the same temperature and same conditions:

$$P(x, T)/P(0, T) = 1 + Ax \tag{1}$$

The slope A is an adjustable parameter used to fit experimental data, which should reflect extrinsic factors such as shapes of tips in addition to intrinsic properties. Using the dimensionless form of the strength aims to minimize the contribution from artifacts such as the processing conditions and the crystal orientation, if the measurement is conducted under the same conditions throughout the course of experiment. The $x = K^{-1/2}$, where $K = R/d$ is the dimensionless form of size, which corresponds to the number of atoms, with mean diameter or bond length d, lined along the radius of a spherical-like nanosolid or across the thickness of a thin film.

The pileup of dislocations at grain boundaries is traditionally envisioned as a key mechanistic process that enhances resistance to plastic flow from grain refinement. As the crystal is refined from the micrometer regime into the nanometer regime, this process invariably breaks down, and the yield strength versus grain size relationship departs markedly from that seen at larger grain sizes. With further grain refinement, the yield stress peaks in many cases at a mean grain size on the order of 10 nm or so. A further decrease in grain size can cause softening of the solid, instead, and then, the HPR slope turns from positive to negative at a critical size, which is called the inverse Hall−Petch relationship (IHPR).[8−13]

There is a concerted global effort underway using a combination of novel processing routes, experimental measurements, and large-scale computations to develop deeper insights into these phenomena. It has been suggested that the grain boundaries consisting of lower coordinated atoms contribute to the grain boundary performance.[14] The strength maximum at a grain size

* E-mail: ecqsun@ntu.edu.sg; fax: 65 6792 0415; http://www.ntu.edu.sg/home/ecqsun/.

† Nanyang Technological University.

‡ The University of New South Wales.

10.1021/jp045894e CCC: $30.25
Published on Web 12/08/2004

of ~10−15 nm for Cu nanosolid is attributed to a switch in the microscopic deformation mechanism from dislocation-mediated plasticity in the coarse-grain interior to the grain boundary sliding in the nanocrystalline regime.[15] A significant portion of atoms resides in the grain boundaries, and the plastic flow of the grain boundary region is responsible for the unique characteristics displayed by such materials.[16] In the HPR regime, crystallographic slips in the grain interiors govern the plastic behavior of the polycrystallite, while in the IHPR regime, grain boundaries dominate the plastic behavior. During the transition, both grain interiors and grain boundaries contribute competitively. The slope in the HPR is suggested to be proportional to the work required to eject dislocations from grain boundaries.[17] Molecular dynamics simulations suggest that the IHPR arises from sliding-accommodated grain boundary diffusion creep.[18] The critical size is suggested to depend strongly on the stacking-fault energy and the magnitude of the applied stress.[19] Unfortunately, an analytical expression for the IHPR transition was absent until recently when Zhao et al.[20] first modified the HPR by introducing the activation energy that can be related directly to the melting point suppression, $T_m(x)$, to the slope A.[21]

Although there is a growing body of experimental evidence pointing to such unusual deformation responses in the nanometer regime, the underlying mechanisms are yet poorly known. As pointed out by Kumar et al.,[22] the physical origin of the IHPR transition has been a long-standing puzzle, and the factors that dominate the critical size at which the HPR transitions occur are far from clear. Here, we show that an extension of the recent practice in dealing with the mechanical strength and compressibility of a monatomic chain[23] has led to an analytical uniscale solution for quantitative information about the unusual mechanical behavior of a surface and a solid over the whole range of sizes, which provides consistent insight into the factors dominating the critical size for IHPR transition and the critical temperature for solid−semisolid transition. Results provide consistent insight into the factors dominating the critical size for IHPR and the critical sizes for solid−semisolid and semisolid−liquid transitions at a given temperature. Agreement also shows that the current model based on bond-order-length−strength (BOLS) correlation is consistent with that derived from the criteria for melting of Lindermann[24] and Born[25] and their derivatives.

II. Principle

2.1. BOLS Correlation. It is worth emphasizing that the termination of the lattice periodicity in the surface normal has two effects: One is the reduction of the coordination numbers (CNs) of the surface atoms and the other is the creation of the surface potential barrier. The potential barrier confines electrons moving inside the solid. According to Goldschmidt[26] and Pauling,[27] if the CN of an atom is reduced, the radius of the lower coordinated atom would shrink spontaneously, disregarding the nature of the specific chemical bond or the dimension or the structural phase of the solid.[28] Therefore, the CN reduction will shorten the remaining bonds of the lower coordinated surface atom with an association of bond strength gain or bond stiffening.[29] However, the atomic cohesive energy that is a production of the bond order and single bond energy would be lowered. The cohesive energy relates directly to the activation energy for thermally activated processes, such as liquidation and evaporation, and mechanically activated processes, such as dislocation of the lower coordinated atoms. This premise has formed the subject of the intensively verified BOLS correlation mechanism that is numerically expressed.[30]

$$\begin{cases} c_i(z_i) = 2\{1 + \exp[(12 - z_i)/(8z_i)]\}^{-1} & \text{(bond contraction coefficient)} \\ E_i = c_i^{-m} E_b & \text{(single bond energy)} \\ E_{bi} = z_{ib} c_i^{-m} E_b & \text{(single atomic cohesion)} \end{cases} \quad (2)$$

The i and b denote an atom in the ith atomic layer and in the bulk. The i is counted from the outermost surface to the central of the solid up to three, as no bond order loss occurs for $i > 3$. The c_i, being the bond contraction coefficient, varies with the effective atomic CN(z_i). The index m, however, discriminates bond nature alteration. Experience revealed that for elemental metals, $m = 1$, for alloys or compounds, $m \approx 4$, and for carbon and silicon, the m has been optimized to be 2.56[31] and 4.88,[32] respectively. The term $z_{ib}c_i^{-m} = E_{Bi}/E_B = z_i/z_b \times E_i/E_b$ is the dimensionless form of atomic cohesive energy being normalized by the bulk value.

Figure 1a shows the CN dependence of the reduced bond length, $c_i(z_i)$.[33] The solid curve formulates the Goldschmidt premise which states that the atomic radius contracts by 12%, 4%, and 3% if the CN of the atom is reduced from 12 to 4, 6, and 8, respectively. Feibelman[34] has noted a 30% contraction of the dimer bond length of Ti and Zr and a 40% contraction of the dimer bond of Vanadium, which is also in line with the formulation. Figure 1b shows the BOLS correlation using the pair interatomic potential, $u(r)$.[23] As the equilibrium atomic distance (bond length) is considered, no particular form of the $u(r)$ is preferred. When the CN of an atom is reduced, the remaining bonds will contract from one (unit in d) to c_i, and the bond energy will increase in magnitude from one (unit in $E_b = E\ (T = 0)$) to c_i^{-m}. As a consequence of the BOLS correlation, densification happens to mass, charge, and energy at sites close to a surface or sites surrounding a structural defect. This understanding may provide a possible atomistic mechanism for the pinning effect of atomic dislocations and atomic voids, of which the energy density rise could substantially strengthen a solid.[35]

The BOLS correlation premise has been widely applied to predicting the tunability of a variety of properties of a nanosolid. Atomic CN imperfection contributes not only to the atomic cohesive energy of the specific discrete atom but also to the energy density in the contracted continuum surface region due to the bond strength gain. Atomic cohesive energy determines the thermodynamic behavior of the system such as critical temperatures for phase transition and solid−liquid transition,[36] as well as the activation energy for atomic diffusion, atomic dislocation, and chemical reaction.[37] The binding energy density perturbs the Hamiltonian of an extended solid that determines the entire band structure such as the band gap expansion,[33] core-level shifts,[29] and bandwidth modification of a nanosolid. The increased energy density in the relaxed surface region enhances the surface stress and the Young's modulus at the surface.[38] Therefore, all the measurable quantities of a nanosolid can be predicted given their functional dependence on bond length, density of mass, charge and energy, or atomic cohesive energy. Most importantly, miniaturizing a solid provides us with a new freedom that not only allows us to tune the physical properties of a solid in a predictable way but also allows us to get quantitative information, such as the energy levels of an isolated atom[29] and the frequency of vibration for an isolated Si−Si dimer,[39] beyond conventional approaches. Extension to the lower end of the size limit has led to the quantification of the strength, extensibility, and thermal stability of a single bond in monatomic chains[23] and the Young's modulus of a C−C bond in carbon

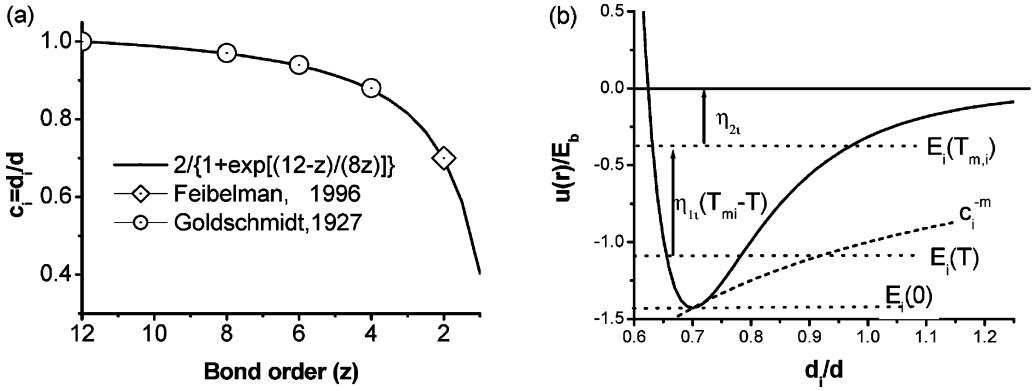

Figure 1. (a) Formulation (solid curve) of the bond order dependence of bond length derived from the Goldshmidt's premise (CN ≥ 4)[26] and Feibelman's notation.[34] (b) Consequence of bond contraction on the binding energy. CN imperfection causes the remaining bonds of the lower-coordinated atom to contract from 1 unit (in d) to c_i, and the cohesive energy per coordinate increases from 1 unit (in E_b) to by c_i^{-m}. Separation between $E_i(T)$ and E_i is the thermal vibration energy. Separation between $E_i(T_{m,i})$ and $E_i(T)$, or $\eta_{1i}(T_{m,i} - T)$, corresponds to energy required for melting, which contributes to the mechanical strength. $T_{m,i}$ is the melting point, which is proportional to the atomic cohesive energy, E_{Bi}. η_{1i} is the specific heat per bond, and η_{2i} is $1/z_i$-fold of energy required for evaporating an atom in the molten state.

nanotubes.[31] Progress made insofar has formed the subject of a recent monographic report.[40]

2.2. Surface Stress and Young's Modulus. One needs to note in Figure 1b that the melting point of the bond between the pairing atoms, $T_{m,i}$, is proportional to the cohesive energy, z_iE_i, of the ith atom with z_i coordinate[21] and that the energy contributing to the mechanical strength at T is the separation between $E_i(T_{m,i})$ and $E_i(T)$, or $\eta_{1i}(T_{m,i} - T)$, as the molten phase is extremely soft and highly compressible.[23,41] η_{1i} is the specific heat per coordinate. The term of $\eta_{1i}(T_{m,i} - T)$, being a portion of the bond energy, E_b, is also $1/z_i$-fold thermal energy required for melting the specific atom. T is the current temperature of operation. Any means that could either raise the T or suppress the $T_{m,i}$ will lower the mechanical strength of the bond. For instance, the $T_{m,i}$ can be reduced by lowering the atomic CN, as $T_{m,i}$ is proportional to the value of z_iE_i. Self-heating during operation may raise the actual temperature of the specimen.

On the other hand, the flow stress or yield strength, being the same in dimension, is the strain-induced energy deviation that is proportional to internal energy density, being the sum of bond energy per unit volume containing N_i atoms.[42] Therefore, the z_i- and T-dependent mechanical strength at the ith atomic site can be expressed as[23]

$$P_i(z_i, T) = -\left.\frac{\partial u(r, T)}{\partial V}\right|_{d_i,T} \approx \begin{cases} \propto \dfrac{N_iE_i(0)}{d_i^3} & (T \ll T_{m,i}) \\ = \dfrac{N_i\eta_{1i}(T_{m,i} - T)}{d_i^3} & \text{(else)} \end{cases} \tag{3}$$

The extensibility or compressibility, β, is the strain divided by the strain-induced stress, which is an inverse of the Young's modulus in dimension and can be expressed as

$$\beta_i(z_i, T) = -\left.\frac{\partial V}{V\partial P}\right|_T = [Y_i(z_i, T)]^{-1} = \left[-V\left.\frac{\partial u^{2^{-1}}(r, T)}{\partial V^2}\right|_T\right]^{-1}$$

$$= \frac{d_i^3}{N_i\eta_{1i}(T_{m,i} - T)} = [P_i(z_i, T)]^{-1} \tag{4}$$

The normalized P_i and Y_i at a specific site share the commonly dimensionless form

$$\frac{P_i(z_i, T)}{P(z_b, T_0)} = \frac{Y_i(z_i, T)}{Y(z_b, T_0)} \begin{cases} \propto c_i^{-(m+3)} & (T \ll T_{m,i}) \\ = \dfrac{\eta_{1i}d^3(T_{m,i} - T)}{\eta_{1b}d_i^3(T_{m,b} - T)} & \text{(else)} \end{cases} \tag{5}$$

The bond number N_i between the circumferential neighboring layers of a nanosolid changes little upon relaxation, and thus, N_i does not come into play upon normalization. The specific heat per bond increases because of bond strength gain. The η_{1i}/η_{1b} value of 3.374 has been obtained for an impurity-free gold monatomic chain.[23] Factors that enhance Y and P are the shortened bond length and the associated energy rise, which is equivalent to $1/z_i$-fold thermal energy required for melting an atom at the initial temperature, T. Therefore, the separation of $T_{m,i} - T$ is crucial to determining the mechanical strength of a specific bond. On the other hand, thermal expansion will contribute to the bond length, which can be expressed as $d_i(z_i, T) = d \times c(z_i)(1 + \alpha T/T_m)$. However, the linear thermal expansion coefficient is in the range of $\alpha \approx 2-4 \times 10^{-7}/T_m$, which can be neglected in numerical calculations compared to the extent of CN-induced bond contraction that is in the 10^{-2} range.

One may note that the Young's modulus is defined for elastic deformation, while its inverse, or the extensibility/compressibility, covers both the elastic and plastic types of deformation. However, either the elastic or the plastic process is related to the process of bond distortion, including bond unfolding, stretching, or breaking, that consumes energy (obtained by integrating the stress with respect to strain) being a certain portion of the entire binding energy. No matter how complicated the actual process of bond deformation (with linear or nonlinear response) or recovery (reversible or irreversible) is, a specific process consumes a fixed portion of bond energy, and the exact portion for the specific process does not come into play in the numerical efforts in seeking for relative change. Therefore, relations 4 and 5 are valid for any substance of any scale of size and in any phase, even liquid and gaseous. As the Young's modulus and mechanical strength are quantities of intensity, they are volumeless. Therefore, it might not be appropriate to think about the stress of a single atom but, instead, the stress at a specific atomic site.

It is important to note that, in the nanoindentation test, errors may arise because of the shapes and sizes of the tips, such as in the cases described in ref 1. In practice, the stress−strain profiles of a nanosolid are not symmetrical when comparing the situation under tension to the situation under compression,[43] and the flow stress is dependent on strain rate, loading mode and time, and materials compactness, as well as size distribution. The hardness of single-crystal moissanite (6H−SiC) obtained by ten-second loading parallel to the crystallographic *c* axis, varies with the loading magnitude. If the load is 0.5 N, the derived hardness is 26 GPa; loading at 29 and 50 N, the corresponding hardnesses are 22.5 and 22 GPa, respectively.[44] It seems that the measured hardness is very complicated, and the hardness of a material is hard to be certain accurately. Fortunately, the effect of tip shape and loading mode never affects the origin and the peaking at the surface in detection. By taking the relative change of the measured quantity into account, artifacts due to the measuring techniques can be minimized in the present approach, seeking for the change relative to the bulk counterpart measured under the same conditions. However, the extrinsic factors could be modeled by changing the prefacer A in the modeling practice. The relative change of intensity, the peak position, and the trend of change could reflect the intrinsic characteristics in physics. Nevertheless, one could not expect to cover fluctuations due to mechanical (strain rate, stress direction, loading mode and time, etc.), thermal (self-heating during process), crystal structure orientation, impurity density, or grain-size distribution effects in a theoretical model, as these fluctuations are extrinsic and hardly controllable. We should focus more on the nature and trend of the unusual behavior in mechanics, as accurate detection of the absolute values remains problematic.[44]

2.3. Nanosolid Mechanics − IHPR. The size and temperature dependence of mechanical strength and compressibility/extensibility of a nansolid can be readily obtained by substituting the size and bond nature dependent $\eta_1(x)$, $d(x)$, and $T_m(x, m)$ for the $\eta_{1i,}$ d_i, and $T_{m,i}$ in eq 5 that are initially derived for a single bond and a flat surface. The derived solution is expressed as

$$\frac{P(x, T)}{P(0, T)} = \frac{\eta_1(x)}{\eta_1(0)}\left(\frac{d(0)}{d(x, T)}\right)^3 \times \frac{T_m(x, m) - T}{T_m(0) - T} = \frac{P(x)}{P(0)}\varphi(d, m, T) \tag{6}$$

The additional term $\varphi(d, m, T)$ covers contributions from bond nature, specific heat, the CN imperfection-induced bond contraction, the T_m suppression, and temperature of operation to the mechanical strength of a solid. The size and bond nature dependent $d(x)$ and $T_m(x, m)$ of a nanosolid have been given in a shell structure as[23,45]

$$\begin{cases} d(x)/d(0) = 1 + \Delta_d(x); & \Delta_d(x) = \sum_{i\le 3}\gamma_i(x) \times (c_i - 1) \\ T_m(x, m)/T_m(0) = 1 + \Delta_B(x, m); & \Delta_B(x, m) = \sum_{i\le 3}\gamma_i(x) \times (z_{ib}c_i^{-m} - 1) \end{cases}$$

$$\gamma_i(x) = \frac{V_i}{V} = \frac{N_i}{N} = \begin{cases} 1 & (K \le 3) \\ \tau c_i x^2 & (\text{else}) \end{cases} \tag{7}$$

where $\Delta_d(x)$ and $\Delta_B(x, m)$ represent the CN imperfection perturbations to the bond length and the atomic cohesive energy, E_B. $\gamma_i(x)$ is the volume or number ratio of atoms in the ith atomic layer over the entire solid, which drops from unity to negligibly small when the solid grows from atomic scale to infinite size. The sum is carried out in a way from bond-by-bond, atom-by-atom, shell-by-shell, to particle-by-particle in a system composed of weakly linked nanosolids, which adequately represents the inhomogeneous features of a shell-structured solid over the whole range of sizes. If one counts atom-by-atom, γ_i exhibits quantized features. For quantities such as the density of charge and energy, one has to consider the continuum form of γ_i by calculating the volumes of different shells. The dimensionality $\tau = 1$, 2, and 3 corresponds to a thin-plate or monatomic chain, a rod, and a spherical dot, respectively.

By comparing the currently derived form (eq 6) with the traditional HPR (eq 1), one can readily find that the ratio of specific heat per bond follows the traditional T unapparent HPR, $\eta_1(x)/\eta_1(0) = P(x, T)/P(0, T) = 1 + Ax$. Incorporating the activation energy, $E_A \propto T_m$,[20,21,46] into the prefector A leads to an analytical expression for the size and temperature-dependent HPR:

$$\begin{aligned} \frac{P(x, T)}{P(0, T)} &= \frac{\eta_1(x)}{\eta_1(0)}\left(\frac{d(0)}{d(x)}\right)^3 \times \frac{T_m(x, m) - T}{T_m(0) - T} \\ &= [1 + A(x, \theta(x), m)] \times \\ &\qquad [1 + \Delta_d(x)]^{-3} \times \frac{T_m(0)[1 + \Delta_B(x, m)] - T}{T_m(0) - T} \\ &= [1 + A(x, \theta(x), m)] \times [1 + \Delta_d(x)]^{-3} \times \\ &\qquad \left[1 + \frac{\Delta_B(x, m)}{1 - \theta(T)}\right] \end{aligned} \tag{8a}$$

where

$$A(x, \theta(x), m) = f \times x \times \exp\left[\frac{T_m(x)}{T}\right] = f \times x \times \exp\left\{\frac{1 + \Delta_B(x, m)}{\theta(T)}\right\} \tag{8b}$$

where $\theta(T) = T/T_m(0)$. The prefactor f is an adjustable parameter, which should represent the contribution from extrinsic factors such as the purity or defect density, shapes of tips, and loading scales to the mechanical strength of a solid. The reduced hardness is a function of the $\theta(T)$, extrinsic factor f, and the bond nature represented by m. Therefore, the competition between bond order loss and bond strength gain intrinsically dictates the IHPR relationship. As the solid size is decreased, transition from the dominance of bond strength gain to dominance of bond order loss happens at the critical size at which both mechanisms contribute competitively. Incorporating the value of $\eta_1(x)/\eta_1(0) = 0.001\,87/0.000\,554\,2 = 3.3742$ for an impurity-free Au monatomic chain[23] into eq 8a, we may estimate the value of f with the parameters of $z_i = 2$, $K = 1.5$, $x = 1/\sqrt{k} = 1/\sqrt{1.5} = 1.225$, $m = 1$, $T = 298$ K, and $T_m(x) = 1337.33/4.1837$:

$$f = 2.3742/\left\{1.225 \times \exp\left[\frac{1337.33}{298 \times 4.1837}\right]\right\} = 0.663 \tag{9}$$

Experimental conditions such as the external stress or strain rate or structural defects will contribute to the mechanical strength through the prefactor $f \approx 0.663$ that is intrinsic for the impurity-free gold. The f value may change upon bond nature alteration, as in the cases of diamond and TiO_2 that will be shown shortly. The analytical form supports for the known grain-interior−grain-boundary transition mechanism for the IHPR[14−17] and further clarifies that the competition between bond order

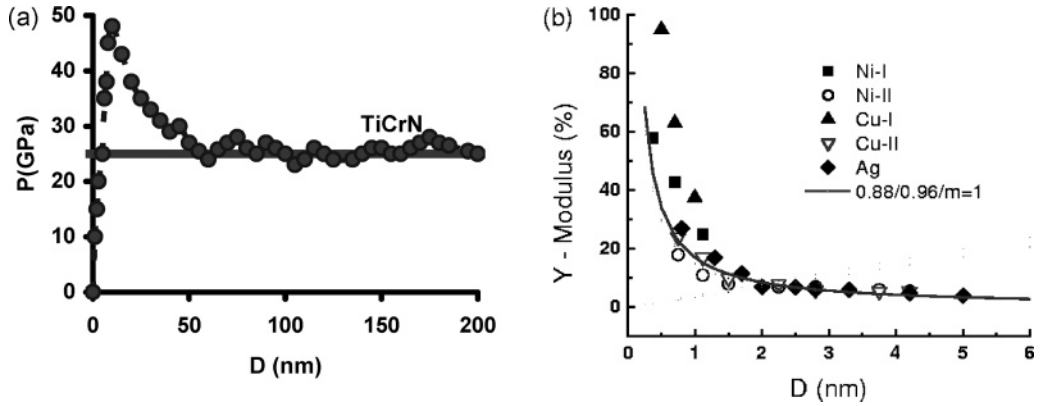

Figure 2. (a) Nanoindentation hardness−depth profile for TiCrN thin film.[38] The peak shift corresponds to the surface roughness (Ra = 10 nm as confirmed by AFM). (b) Agreement between predictions and measured size dependence of the Young's modulus of Ni-I and Cu-I,[49] Ni-II, Cu-II, and Ag[50] thin films.

loss and bond strength gain dictates the mechanical behavior at grain boundaries. According to this solution, grain boundary is harder at temperatures far below $T_m(x, m)$ because of the dominance of bond strength gain, whereas at temperatures close to $T_m(x, m)$, the grain boundary is softer than the grain interior because of the bond order loss that lowers the barrier for atomic dislocation. If operating at a given temperature, solid size reduction causes a reduction in $T_m(x, m)$. When x approaches zero, the analytical form converges to the traditional HPR, of which the slope is clarified herein to be dominated by the term $f \times \exp[T_m(0)/T]$ that relates to the specific heat or activation energy for atomic dislocation.

2.4. Critical Sizes for IHPR Transition. By solving the relation $d[Ln(P/P_0)]/dx = 0$ (eq 6), we can readily find the critical size $x_C[f, \theta(T), m]$ and, hence, the factors dominating x_C. P and P_0 represent $P[x, \theta(T)]$ and $P[0, \theta(T)]$, respectively. The numerical process leads to the following relation

$$\frac{d[Ln(P/P_0)]}{dx} = A[x, \theta(x), m] \times \frac{\theta(0) + 2\Delta_B(x, m)}{\theta(0)\{1 + A[x, \theta(x), m]\}} - \frac{6\Delta_d(x)}{1 + \Delta_d(x)} + \frac{2\Delta_B(x, m)}{1 + \Delta_B[x, \theta(x), m] - \theta(0)} = 0 \quad (10)$$

2.5. T_C for Solid−Semisolid and Semisolid−Liquid Transition. We may define the critical temperature, T_C, for the solid−semisolid and semisolid−liquid transition by the relation

$$\frac{P(x, T_C)}{P(0, T_C)} = \frac{1 + A[x, \theta(T_C), m]}{[1 + \Delta_d(x)]^3} \times \left[1 + \frac{\Delta_B(x, m)}{1 - \theta(T_C)}\right] = \begin{cases} 1 & \text{(semisolid)} \\ 0 & \text{(liquid)} \end{cases} \quad (11)$$

At temperatures higher than $T_C(x, f, m)$, the solid is softer and easily compressible compared with the bulk counterpart at the same temperature. At the melting point, $T_m(x, m)$, the semisolid-to-liquid transition happens, associated with zero hardness and infinity compressibility. This definition is quite the same as that of Born's criterion indicating that the shear modulus of a solid approaches zero when the solid melts.[25]

III. Results and Discussion

3.1. Surface Mechanics. An examination of the hardness and Young's modulus using nanoindentation revealed that the surface of TiCrN thin films[38] reaches a maximum of 100% higher than its bulk value, as shown in Figure 2a. The same trend holds for amorphous carbon[47] and AlGaN[48] films with peaks positioned at several nanometers' depth that corresponds to the surface roughness. Solving eq 5 with the measured value of $\Delta P/P = (50 - 25)/25 = 1$ gives rise to c_i values of 0.883 associated with $m = 4$. Figure 2b shows consistency between BOLS predictions and the theoretically calculated thickness dependence of Young's modulus for Ni, Cu, and Ag thin films.[49,50] BOLS predictions were obtained by summing eq 5 over the top three atomic layers with $z_1 = 4$, $z_2 = 6$, and $m = 1$ for the pure metals. It is interesting to note that at the thinnest limit (two atomic layers), the Young's modulus of Cu is 100% higher than the bulk value, which agrees with that detected from the surface of TiCrN,[38] α_2-TiAl and γ-TiAl films.[3] Correlation between the maximal Y values and the lattice contraction of Liu et al.[6] leads to c_i of 94.8% for steel, which agrees with the BOLS low-T prediction of $Y_i/Y_b = c_i^{-(m+3)}$ with $m = 1$ for metals.

However, the high $P_i/P > 2$ values for Ag, Ni, Cu, and Al thin films[3] and amorphous carbon films[2] are beyond the BOLS expectation. The unexpected high surface hardness may be a contribution from tip shapes or loading scales as discussed already.[1,44] Structural defects also contribute to the mechanical strength of a solid.[35] For instance, the internal stress of amorphous carbon films can be modulated by changing the sizes of nanopores that are produced by the bombardment of noble gases (Ar, Kr, and Xe).[51,52] When ~1−11 GPa internal stress is generated by controlling the size of the pores within which noble gases are trapped, the core-level binding energy of the entrapped gases is lowered by ~1 eV associated with 0.05 nm expansion of the atomic distance of the noble gases. For Ar (Xe), the first interatomic separation varies from 0.24 (0.29) nm to 0.29 (0.32) nm in the 1−11 GPa pressure range. The binding energy weakening and atomic distance expansion of the trapped gases indicate clearly that the gas-entrapped pores expand and the interfacial C−C bonds contract, which contribute to the extraordinary mechanical strength of the thin films.

3.2. Nanosolid IHPR. Further calculations using eq 8a were performed on some nanosolids with known d and T_m values as input and x_C as output shown in Table 1. All the nanograins were taken as spherical-shaped. The size-dependent $d(x)$ and $T_m(x, m)$ values have been determined in refs 23 and 45 by taking the atomic CN of the three outermost atomic layers of the spherical dot as $z_1 = 4(1 - 0.75x^2)$, $z_2 = 6$, and $z_3 = 12$. The prefector f is adjusted under the constraint that the slope should match the observations and intercept at the positive side of the vertical axis. A negative intercept in measurement is physically unacceptable. The theoretical curves were normalized

TABLE 1: Prediction of the Critical Sizes for IHPR Transition with $f = 0.5$, 0.663 and $m = 1$ Otherwise as Indicated[a]

element	d/nm	T_m/K	P_M	measured D_C/nm	predicted D_C/nm ($f = 0.5$; 0.663)
Mg	0.32	923			18.2; 17.3
Ca	0.394	1115			22.41; 22.41
Ba	0.443	1000			25.2; 23.9
Ti	0.293	1941			23.6; 23.6
Zr	0.319	2182			29.3; 29.3
V	0.2676	2183			24.6;24.6
Ta	0.2914	2190			26.8;26.8
Fe	0.252	1811	9765	18.2	19.1
Co	0.2552	1728			19.3
Ni	0.2488	1728	7042	17.5	18.8
Cu	0.2555	1358	890	14.9	16.1
Zn	0.2758	693	1034	17.2	18.5; 16.5
Pd	0.2746	1825	3750	19.9	20.8
Ag	0.2884	1235			17.3
Pt	0.277	1828			21.0
Au	0.288	1337			17.3
Al	0.286	993			16.3;15.4
C	0.154	3800			20.5 ($m = 2.56$)
Si	0.2632	1683	4	9.1 ($m = 4.88$, $f = 0.1$)	10.6
Ge	0.2732	1211		($m = 4.88$, $f = 0.1$)	11.5
Sn	0.384	505.1			47.2; 40.6
Pb	0.3492	600.6			28.0; 24.9
Bi	0.34	544.4			36.0; 29.2
$Ni_{80}P_{20}$	0.2429	1184	7063	7.9 ($m = 4$)	8.9
$NiZr_2$	0.4681	1393	7093	17.0 ($m = 4$)	19.8
TiO_2	0.3860	2098	7432	22.5 ($m = 4$)	23.1($f = 0.01$)

[a] The predicted critical sizes agree with the measurements. Changing the f value only affects the D_C of a low-T_m material.

with the calculated peak values at x_C, and the experimental data measured at room temperature were normalized with the measured maximum P_M.

Typical results are compared in Figure 3 for (a) Cu,[53−55] (b) Fe,[53] (c) Ni,[11,56] (d) NiP,[57] and NiZr,[12] (e) TiO_2,[58] and (f) Si.[5] The straight lines are the traditional HPR, and its slope is obtained by adjusting the f values in eq 8a. The solid lines are the current predictions without using any other adjustable parameters. The dashed lines only consider the contribution from the activation energy with $\varphi(d, m, T) = 1$, being quite similar to the approach of Zhao et al.[20] The scattered data are experimental results from different sources. All the panels were fitted at $T = 300$ K, with $f = 0.5$ otherwise as indicated. The BOLS predictions match reasonably well to all measurements compared with the approach with $\varphi(d, T, m) = 1$. The perfect match of NiP alloy may evidence adequately the current BOLS approach that is close to the true situations of IHPR. As can be seen from Table 1, changing the f values from 0.5 to 0.663 has no effect on the critical size for materials with $T_m(0) > 1000$ K, and therefore, for the examined samples, there is no difference using $f = 0.5$ versus 0.663. The small f values for TiO_2 (0.01) and diamond (0.1) may be dominated by the bond nature alteration that raises the $T_m(x, m)$.

Strikingly, a single measurement is sufficient to calibrate the IHPR of a specific solid. Applying the relative hardness of the defect-free 40 nm silicon nanosphere[5] to the IHPR equation results in the maximal hardness of Si nanosolid at room temperature being 5 times the bulk value and the IHPR critical size being ~9−10 nm. The calibration using a single data point should be one of the advantages of the current approach in revealing and calibrating the IHPR of any solid. Applying $m = 4.88$ for Si to eq 8a immediately gives $c_1 = (15 \pm 1)\%$ and the corresponding $z_1 \approx 3.60 \pm 0.25$. The z_1 value is slightly lower than $z_1 = 4$ for a flat surface, and the c_1 value is slightly higher than that of the TiCrN flat surface $(13 \pm 1)\%$ because of the curvature of the sphere.

3.3. Factors Dominating the Critical Size. Figure 4 compares the size dependence of the ductility (broken lines) and IHPR-2 (solid lines) of (a) Pb ($m = 1$, $T_m = 600.6$ K, $f = 0.663$) and (b) Au ($m = 1$, $T_m = 1337.33$ K, $f = 0.663$) operated at 300 K. The ratio $P(x)/P(0) = 1$ corresponds to the critical temperature for solid−semisolid transition; $P(x)/P(0) = 0$ corresponds to the temperature for semisolid−liquid transition. The reduced compressibility drops first, then bends up at the IHPR critical size until the bulk value at $T_C(x)$, and then goes up to infinity at $T_m(x)$. Results show that Pb nanosolid of $x = 0.34$ ($D = 6$ nm) size becomes semisolid and that of $x = 0.52$ (2.6 nm) becomes liquid at 300 K; Au nanosolid of $x = 0.68$ ($D = 1.25$ nm) becomes semisolid. The Au monatomic chain (monatomic chain, MC, with $K = 1.5$) is in a semisolid state, which further clarifies the high extensibility of gold MC at the ambient temperature.[23] IHPR-1 with $\varphi(x, m, T) = 1$ could hardly reach the semisolid or liquid state in both cases.

Figure 5 examines the f, m, and $T/T_m(0)$ dependence of the x_C values. The critical size varies significantly with the $T/T_m(0)$ ratio and the m value as well. In the range of $f \approx 0.1-1.0$, x_C depends less on the f values if the $T/T_m(0)$ ratio is smaller than 0.2.

3.4. Size Effect on $T_C(x)$ and $T_m(x)$. From the T/T_m and size dependence of strength and ductility in Figure 6a, we may note the following trends in general: (i) For a given material of a given size, the normalized mechanical strength drops from infinity to zero when T approaches $T_m(x, m)$, associated with increases of ductility that approach infinity at the $T_m(x)$ value that drops by 5% and 15%, respectively, for $x_C = 0.15$ and 0.21. (ii) Both P and β reach their bulk values at $T_C = 0.75T_m$ and $0.65T_m$ for $x_C = 0.15$ and 0.21, respectively. When $T > T_C$, P drops and β rises in an exponential way. A comparison of the size dependence of the normalized atomic distance $d(x)/d(0)$, melting point, $T_m(x, m = 1)/T_m(0)$, and $T_C(x, f, m = 1)/T_m(0)$ for solid-to-semisolid transitions shown in Figure 6b indicates that $T_C(x, f)$ drops more rapidly with size than $T_m(x, m)$. The bulk $T_C(0)$ value is about 20% lower than the bulk melting point. It is interesting to note that the $T_m(x)/T_m(0)$-I curve derived from the BOLS correlation overlaps the $T_m(x)/T_m(0)$-II curve, indicating the consistency in the respective physical mechanisms of melting. The former represents that the melting point is governed by the atomic cohesive energy, and the latter representing eq 11 means that at the melting point the mechanical strength is zero, the same as Born's criterion which indicates that at the melting point, the shear modulus approaches zero.[25] The two curves also agree with the model of Jiang et al. derived from Lindermann's criterion of atomic vibration and its derivatives of surface lattice/phonon instability.[59−61]

For a Cu nanosolid with $K = 10$ (5 nm in diameter) as a sample, the bond contracts by a mean value of 5%, associated with a 25% drop of T_m and a 50% drop of T_C with respect to the bulk $T_m(0)$ (1358 K). The 5 nm-sized nanosolid is in a semisolid state at 680 K. The self-heating in operation due to bond-breaking that releases energy should raise the actual temperature of the specimen substantially. Hence, the size-induced T_C drop and the self-heating in operation may provide an additional mechanism for the high ductility of Cu nanowires at ambient temperatures.[62]

The predicted m, f, and $T/T_m(0)$ dependence of x_C and $T_C(x)$ and the trends of mechanical strength and compressibility/extensibility coincide exceedingly well with the cases as reported by Eskin, Suyitno, and Katgerman[41] on the grain size depen-

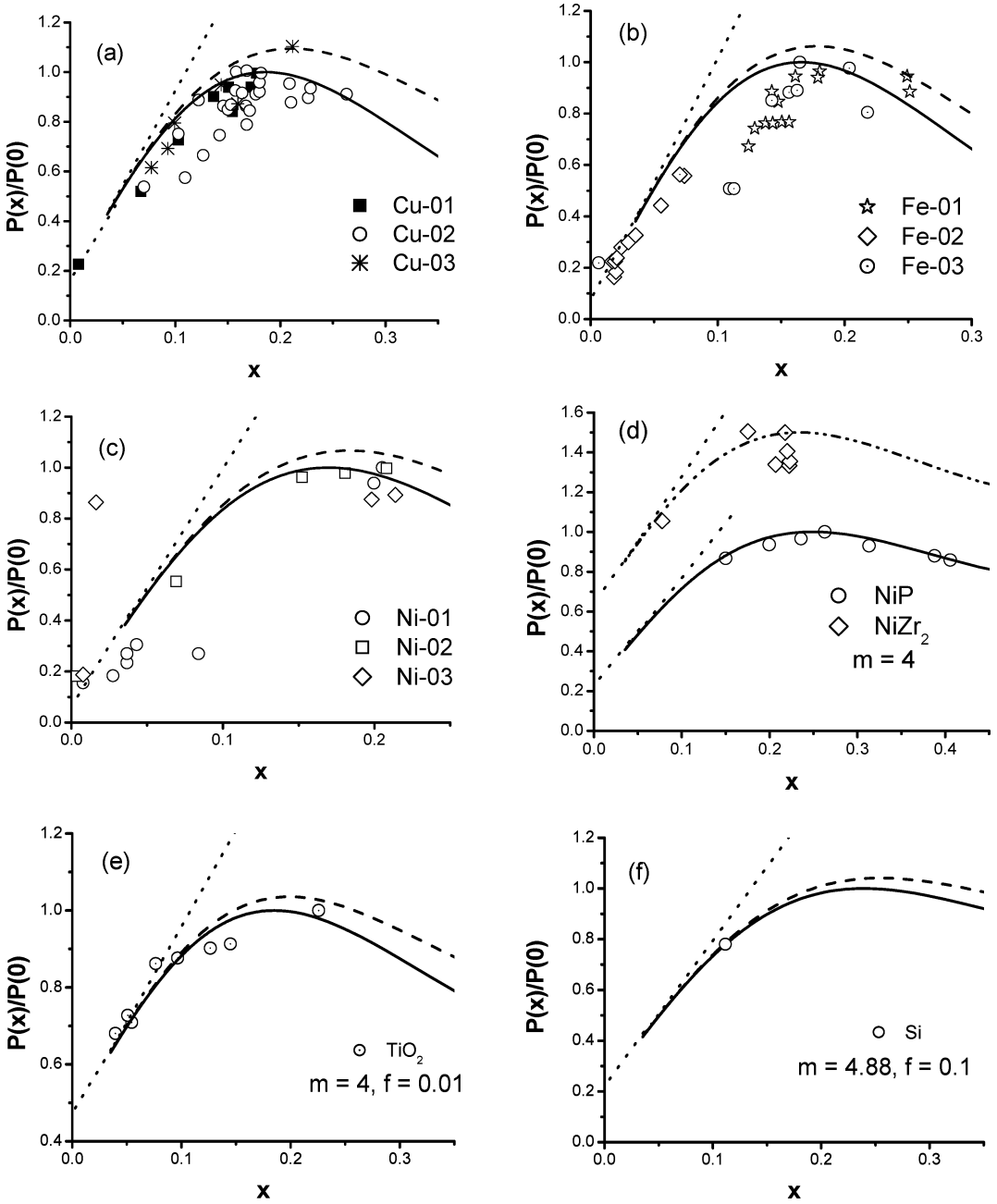

Figure 3. Comparison of the calculated (solid line) with the measured IHPR (scattered data) values of (a) Cu,[53,54,55] (b) Fe,[53] (c) Ni,[56] (d) NiP[57] and $NiZr^{12}$ (e) TiO_2,[58] and (f) Si.[5] The solid curves represent the complete BOLS form of $[1 + f \times x \times \exp(T_m(x)/T)]\varphi(d, m, T)$. The straight lines are traditional HPR representing $1 + f \times x \times \exp(T_m(0)/T)$, and its intercept at the *y*-axis corresponds to the normalized hardness of the bulk counterparts. The dashed curved lines are the modified HPR with $[1 + f \times x \times \exp(T_m(x)/T)]$. The slope $f = 0.5$ was optimized otherwise as indicated for all samples.

dence of the tensile elongation (extensibility) of an $Al_{0.04}Cu$ alloy in the semisolid state. The ductility increases exponentially with temperature until infinity at T_m that drops with solid size. On the other hand, the ductility increases generally with grain refinement. This is also the frequently observed case such as the size-enhanced compressibility of alumina[63] and PbS[64] in nanometer range at room temperature.[65,66] The predicted trends also agree with experimental observations[67] of the temperature dependence of the yield stress of Mg nanosolids of a given size showing that the yield strength drops as the operating temperature rises. An atomic-scale simulation[68] also suggests that the material becomes softer in both the plastic and elastic regimes as the operating temperature is raised. When measuring at 200 °C, the strength of 300-nm-sized Cu nanograins is lowered by 15% and the ductility increases substantially.[69] Temperature dependence of the tensile properties of ultrafine-grained ordered FeCo−2V samples with grain sizes of 100, 150, and 290 nm revealed that extremely high yield strengths (up to 2.1 GPa) are present at room temperature with appreciable ductility of ∼3−13%. The measured strengths declined gradually as the testing temperature was increased to 400 °C, while ductility was generally enhanced, up to 22%.[70] Consistency between BOLS predictions and experimental observations sufficiently show that the *m* and T/T_m dependent compressibility and strength describes the true situation. Given the bulk melting point and the atomic size, it is easy to predict the critical size for the IHPR transition and the critical T_C for the solid−semisolid transition of a solid. As listed in Table 1, the predicted critical size at room temperature is within ∼8−35 nm, agreeing surprisingly well with documented data.

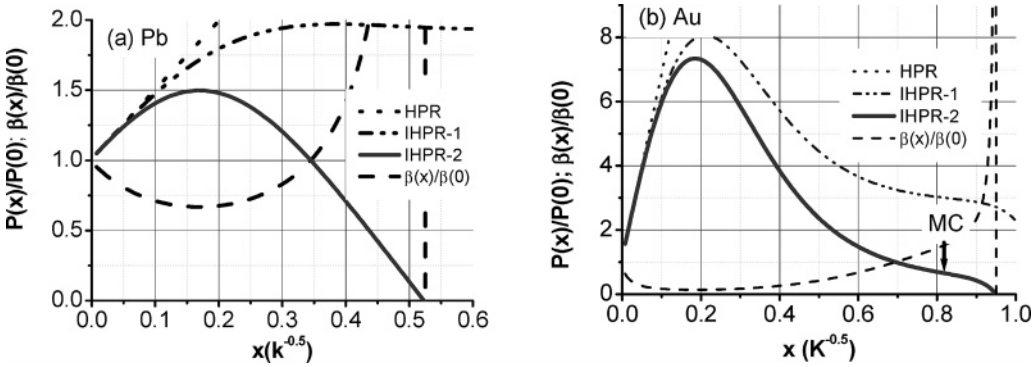

Figure 4. Comparison of the IHPR-2 (solid line) transition and critical sizes for solid-to-semisolid and semisolid−liquid transition at 300 K for (a) Pb ($m = 1$, $T_m = 600.6$ K, $f = 0.663$) and (b) Au ($m = 1$, $T_m = 1337.33$ K, $f = 0.663$). $P/P_0 = 1$ corresponds to semisolid state with critical temperature $T_C(x)$; $P/P_0 = 0$ corresponds to semisolid−liquid transition $T_m(x)$. Broken line represents the reduced compressibility that drops first, then bends up until the bulk value at $T_C(x)$, and then goes up to infinity at $T_m(x)$. Pb nanosolid of $x = 0.34$ ($D = 6$ nm) size becomes semisolid and $x = 0.52$ (2.6 nm) becomes liquid at 300 K; Au nanosolid of $x = 0.68$ ($D = 1.25$ nm) becomes semisolid. The Au monatomic chain (MC with $K = 1.5$) is in semisolid state, which clarifies further the high extensibility of gold MC at the ambient temperature.[23] IHPR-1 could not reach the semisolid or liquid state.

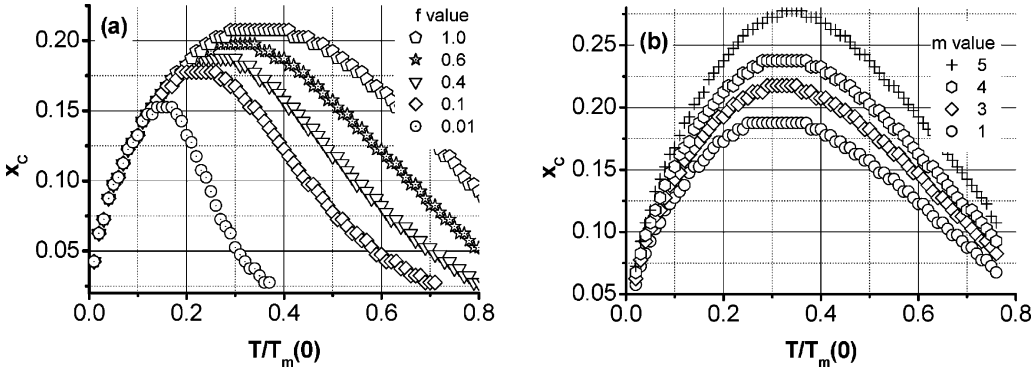

Figure 5. Dependence of x_C (m, f, $T/T_m(0)$) on (a) extrinsic factor f and (b) bond nature recognized with m values.

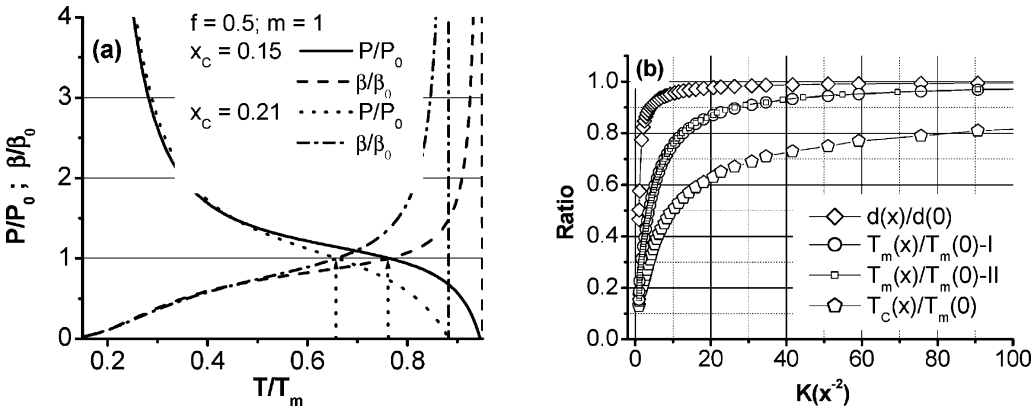

Figure 6. (a) The T/T_m ratio dependent strength and ductility of size x_C values of 0.15 and 0.21, and (b) comparison of size dependence of critical temperature for solid−semisolid transition, $T_C(x)/T_m(0)$, bond length contraction, $d(x)/d(0)$, and semisolid−liquid transition of metallic nanosolid ($m = 1$). $T_m(x)/T_m(0)$-I (BOLS prediction) curve overlaps the $T_m(x)/T_m(0)$-II (Born's criterion).

IV. Conclusion

We have derived an atomistic, uniscale solution to the mechanical strength of a surface and a solid over the whole range of sizes on the basis of the recent BOLS correlation mechanism and the following facts as physical constraints: (i) mechanical enhancement happens at the site surrounding a defect or at a surface because of the CN imperfection-enhanced bond strength gain; (ii) the molten phase is extremely soft and highly compressible; (iii) atomic dislocation at the grain boundary requires activation energy that is proportional to the melting point; (iv) activation energy for atomic dislocation drops because of the bond order loss. Matching predictions to observations reveals the following:

(i) A surface is harder at temperatures far below T_m, but the surface melts more easily compared to the bulk interior. The temperature separation ($T_m - T$) cannot be neglected in dealing with the mechanical strength and ductility of a nanosolid.

(ii) The IHPR originates from the competition between the bond order loss and the associated bond strength gain near the surface edges. As solid size decreases, a transition from dominance of bond strength gain to dominance of bond order loss occurs at the IHPR critical size because of the increased portion of lower coordinated atoms. During the

transition, both bond order loss and bond strength gain contribute competitively.

(iii) The IHPR critical size is universally predictable, which can be calibrated with a few measured data points for a specific system. The critical size is dominated intrinsically by bond nature and T/T_m ratio and extrinsically by experimental conditions or other factors such as size distribution and impurities that are represented by the factors f's.

(iv) The IHPR at larger solid size converges to the normal HPR that holds its conventional meaning of the accumulation of atomic dislocations that resists further atomic displacements in plastic deformation. The slope in the traditional HPR is proportional to $\exp(T_m/T)$, which addresses the relationship between the hardness and the activation energy for atomic dislocations. The x in the conventional HPR should represent the accumulation of atomic dislocations that resists further dislocations, and the constant f may describe the contribution from extrinsic factors such as the shapes of tips, loading scales, strain rates, and defect intensity.

(v) Understanding should provide an additional mechanism for the high ductility of a metallic nanosolid as the critical temperature for the solid-to-semisolid transition is much lower than the bulk melting point, and self-heating should raise the real temperature of the small samples.

Consistency between predictions and observations, together with progress made by the practitioner and co-workers, further evidence the impact of atomic CN imperfection to the mechanical strength and ductility of a nanosolid and the validity and essentiality of the BOLS correlation mechanism and the associated approaches. Therefore, no multiscale approaches are necessary in the current "bottom up" exercise.

Acknowledgment. Helpful discussions with Stan Veprek and John S. Colligon and S.R.P. Silva are gratefully acknowledged.

References and Notes

(1) Mirshams, R. A.; Parakala, P. *Mater. Sci. Eng., A* **2004**, *372*, 252.
(2) Liu, E.; Shi, X.; Tan, H. S.; Cheah, L. K.; Sun, Z.; Tay, B. K.; Shi, J. R. *Surf. Coat. Technol.* **1999**, *20*−*121*, 601.
(3) Zhao, M.; Slaughter, W. S.; Li, M.; Mao, S. X. *Acta Mater.* **2003**, *51*, 4461.
(4) Ferro, D.; Teghil, R.; Barinov, S. M.; D'Alessio, L.; DeMaria, G. *Mater. Chem. Phys.* **2004**, *87*, 233.
(5) Gerberich, W. W.; Mook, W. M.; Perrey, C. R.; Carter, C. B.; Baskes, M. I.; Mukherjee, R.; Gidwani, A.; Heberlein, J.; McMurry, P. H.; Girshick, S. L. *J. Mech. Phys. Solids* **2003**, *51*, 979.
(6) Liu, M.; Shi, B.; Guo, J.; Cai, X.; Song, H. *Scr. Mater.* **2003**, *49*, 167.
(7) Hall, E. Q. *Proc. R. Soc. London* **1951**; B64, 747. Petch, N. J. *J. Iron. Steel Inst.* **1953**, *174*, 25. Ashby, M. F. *Philos. Mag. A* **1982**, *46*, 737.
(8) Wang, Y. M.; Chen, M. W.; Zhou, F. H.; Ma, E. *Nature (Londen)* **2002**, *419*, 912.
(9) Jang, D.; Atzmon, M. *J. Appl. Phys.* **2003**, *93*, 9282.
(10) Conrad, H.; Narayan, J. *Appl. Phys. Lett.* **2002**, *81*, 2241.
(11) Kim, H. S. *Scri. Mater.* **1998**, *39*, 1057.
(12) Lu, K. *Mater. Sci. Eng.* **1996**, *R16*, 61.
(13) Van Swygenhoven, H.; Derlet, P. M.; Hasnaoui, A. *Phys. Rev. B* **2002**, *66*, 024101.
(14) Cheng, S.; Spencer, J. A.; Milligan, W. W. *Acta Mater.* **2003**, *51*, 4505.
(15) Schiøtz, J.; Jacobsen, K. W. *Science* **2003**, *301*, 1357.
(16) Jiang, B.; Weng, G. J. *J. Mech. Phys. Solids* **2004**, *52*, 1125.
(17) Bata, V.; Pereloma, E. V. *Acta Mater.* **2004**, *52*, 657.
(18) Wolf, D.; Yamakov, V.; Phillpot, S. R.; Mukherjee, A. K. *Z. Metallkd.* **2003**, *94*, 1091.
(19) Yamakov, V.; Wolf, D.; Phillpot, S. R.; Mukherjee, A. K.; Gleiter, H. *Nat. Mater.* **2004**, *3*, 43.
(20) Zhao, M.; Li, J. C.; Jiang, Q. *J. Alloys Compd.* **2003**, *361*, 160.
(21) Kocks, U. F.; Argon, A. S.; Ashby, A. S. *Prog. Mater. Sci.* **1975**, *19*, 1.
(22) Kumar, K. S.; Van Swygenhoven, H.; Suresh, S. *Acta Mater.* **2003**, *51*, 5743.
(23) Sun, C. Q.; Li, C.; Li, S.; Tay, B. K. *Phys. Rev. B* **2004**, *69*, 245402.
(24) Lindemann, F. A. *Z. Phys.* **1910**, *11*, 609.
(25) Born, M. *J. Chem. Phys.* **1939**, *7*, 591.
(26) Goldschmidt, V. M. *Ber. Dtsch. Chem. Ges*. **1927**, *60*, 1270.
(27) Pauling, L. *J. Am. Chem. Soc.* **1947**, *69*, 542.
(28) Sinnot, M. J. *The solid state for Engineers*; Wiley & Sons: New York, 1963
(29) Sun, C. Q. *Phys. Rev. B* **2004**, *69*, 045105.
(30) Sun, C. Q.; Zhong, W. H.; Li, S.; Tay, B. K.; Bai, H. L.; Jiang, E. Y. *J. Phys. Chem. B* **2004**, *108*, 1080.
(31) Sun, C. Q.; Bai, H. L.; Tay, B. K.; Li, S.; Jiang, E. Y. *J. Phys. Chem. B* **2003**, *107*, 7544.
(32) Sun, C. Q.; Pan, L. K.; Fu, Y. Q.; Tay, B. K.; Li, S. *J. Phys. Chem. B* **2003**, *107*, 5113.
(33) Sun, C. Q.; Chen, T. P.; Tay, B. K.; Li, S.; Huang, H.; Zhang, Y. B.; Pan, L. K.; Lau, S. P.; Sun, X. W. *J. Phys. D* **2001**, *34*, 3470.
(34) Feibelman, P. *J. Phys. Rev. B* **1996**, *53*, 13740.
(35) Kettle, C. *Introduction to Solid State Physics*, 6th ed.; Wiley: New York, 1986.
(36) Sun, C. Q.; Wang, Y.; Tay, B. K.; Li, S.; Huang, H.; Zhang, Y. *J. Phys. Chem. B* **2002**, *106*, 10701.
(37) Sun, C. Q.; Pan, L. K.; Bai, H. L.; Li, Z. Q.; Wu, P.; Jiang E. Y. *Acta Mater.* **2003**, *51*, 4631.
(38) Sun, C. Q.; Tay, B. K.; Lau, S. P.; Sun, X. W.; Zeng, X. T.; Bai, H. L.; Liu, H.; Liu, Z. H.; Jiang, E. Y. *J. Appl. Phys.* **2001**, *90*, 2615.
(39) Pan, L. K.; Sun, C. Q.; Li, C. M. *J. Phys. Chem. B* **2004**, 108, 3404.
(40) Sun, C. Q. Nanosolid Physics, bond order-length-strength (BOLS) correlation mechanism for the significance of atomic coordination number imperfection; submitted for publication.
(41) Eskin, D. G.; Suyitno; Katgerman, L. *Prog. Mater. Sci.* **2004**, *49*, 629.
(42) Sun, C. Q. *Prog. Mater. Sci.* **2003**, *48*, 521.
(43) Lund, A. C.; Nieh, T. G.; Schuh, C. A. *Phys. Rev. B* **2004**, *69*, 012101.
(44) Brazhkin, V.; Dubrovinskaia, N.; Nicol, M.; Novikov, N.; Riedel, R.; Solozhenko, V.; Zhao, Y. *Nat. Mater.* **2004**, *3*, 576
(45) Sun, C. Q.; Li, S.; Tay, B. K. *Appl. Phys. Lett.* **2003**, *82*, 3568.
(46) Qin, X. Y.; Zhu, X. G.; Gao, S.; Chi, L. F.; Lee, J. S. *J. Phys.: Condens. Matter* **2002**, *14*, 2605.
(47) Shi, X.; Tay, B. K.; Flynn, D. L.; Sun, Z. *Mater. Res. Soc. Symp. Proc.* **1997**, *436*, 293.
(48) Caceres, D.; Vergara, I.; Gonzalez, R.; Monroy, E.; Calle, F.: Munoz, E.: Omnes, F. *J. Appl. Phys.* **1999**, *86*, 6773.
(49) Dodson, B. W. *Phys. Rev. Lett.* **1998**, *60*, 2288.
(50) Streitz, F. H.; Cammarata, R. C.; Sieradzki, K. *Phys. Rev. B* **1994**, *49*, 10699.
(51) Lacerda, R. G.; Dos Santos, M. C.; Tessler, L. R.; Hammer, P.; Alvarez, F.; Marques, F. C. *Phys. Rev. B* **2003**, *68*, 054104.
(52) Poa, C. H. P.; Lacerda, R. G.; Cox, D. C.; Silva, S. R. P.; Marques, F. C. *Appl. Phys. Lett.* **2002**, *81*, 853.
(53) Sanders, P. G.; Eastman, J. A.; Weertman, J. R. *Acta Mater.* **1997**, *45*, 4019.
(54) Fu, H. H.; Benson, D. J.; Meyers, M. A. *Acta Mater.* **2001**, *49*, 2567.
(55) Sanders, P. G.; Youngdahl, C. J.; Weertman, J. R. *Mater. Sci. Eng.* **1997**, *A234*−*236*, 77.
(56) Schuh, C. A.; Nieh, T. G.; Yamasaki, T. *Scr. Mater.* **2002**, *46*, 735.
(57) Palumbo, G.; Erb, U.; Aust, K. T. *Scr. Metall. Mater.* **1990**, *24*, 2347.
(58) Höfler, H. J.; Averback, R. S. *Scr. Metall. Mater.* **1990**, *24*, 2401.
(59) Jiang, Q.; Zhang, Z.; Li, J. C. *Chem. Phys. Lett.* **2000**, *322*, 549.
(60) Shi, F. G. *J. Mater. Res.* **1994**, *9*, 1307.
(61) Vallee, R.; Wautelet, M.; Dauchot, J. P.; Hecq, M. *Nanotechnology* **2001**, *12*, 68.
(62) Lu, L.; Sui, M. L.; Lu, K. *Science* **2000**, *287*, 1463.
(63) Chen, B.; Penwell, D.; Benedetti, L. R.; Jeanloz, R.; Kruger, M. B. *Phys. Rev. B* **2002**, *66*, 144101.
(64) Qadri, S. B.; Yang, J.; Ratna, B. R.; Skelton, E. F.; Hu, J. Z. *Appl. Phys. Lett.* **1996**, *69*, 2205.
(65) Gallas, M. R.; Piermarini, G. J. *J. Am. Ceram. Soc.* **1994**, *77*, 2917.
(66) Zhao, J.; Hearne, G. R.; Maaza, M.; Laher-Lacour, F.; Witcomb, M. J.; Bihan, T. L.; Mezouar, M. *J. Appl. Phys.* **2001**, *90*, 3280.
(67) Ono, N.; Nowak, R.; Miura, S. *Mater. Lett.* **2004**, *58*, 39.
(68) Schiotz, J.; Vegge, T.; Di Tolla, F. D.; Jacobsen, K. W. *Phys. Rev. B* **1999**, *60*, 11971.
(69) Krasilnikov, N. A.; Pakiela, Z.; Lojkowski, W.; Valiev, R. Z. *Solid State Phenom.* **2003**, *94*, 51−54.
(70) Duckham, A.; Zhang, D. Z.; Liang, D.; Luzin, V.; Cammarata, R. C.; Leheny, R. L.; Chien, C. L.; Weihs, T. P. *Acta Mater.* **2003**, *51*, 4083.